

Some computational results for $\mathbf{P}_1 - P_1$ and $\mathbf{P}_2 - P_1$ Trace FEM for the surface Stokes problem

Alexander Zhiliakov*

July 16, 2019

Contents

1 Preliminaries	2
1.1 Bilinear forms and matrices	2
1.2 Quadratures for bilinear forms	3
1.3 Error computation	6
2 Convergence results	6
2.1 Manufactured solution	6
2.2 $P_2 - P_1$ Trace FEM	8
2.2.1 Inconsistent penalty formulation	8
2.2.2 Consistent penalty formulation	9
3 Inf-sup stability: pressure Schur complement generalized eigenvalues	9
3.1 Solution description	9
3.2 Dependency of the spectrum on the mesh size	11
3.3 Sensitivity of the spectrum to levelset shifts	12

*Department of Mathematics, University of Houston, Houston, Texas 77204 (alex@math.uh.edu).

1 Preliminaries

1.1 Bilinear forms and matrices. We set $n_{\mathbf{A}}$ to be the number of velocity d.o.f. and $n_{\mathbf{S}}$ to be the number of pressure d.o.f. Vector stiffness, divergence, pressure mass, normal stabilization, and full stabilization matrices resulting from Trace FEM discretization of the surface Stokes problem [2] are defined via

$$\begin{aligned}
 \langle \mathbf{A} \vec{\mathbf{u}}, \vec{\mathbf{v}} \rangle &\approx \int_{\Gamma} \left(2 E_{s,\Gamma}(\mathbf{u}) : E_{s,\Gamma}(\mathbf{v}) + \mathbf{u} \cdot \mathbf{v} + \tau (\mathbf{u} \cdot \mathbf{n}_{\Gamma}) (\mathbf{v} \cdot \mathbf{n}_{\Gamma}) \right) ds \\
 &\quad + \rho_u \int_{\Omega_h^{\Gamma}} \frac{\partial \mathbf{u}}{\partial \mathbf{n}_{\Gamma}} \cdot \frac{\partial \mathbf{v}}{\partial \mathbf{n}_{\Gamma}} dx, \quad \mathbf{A} \in \mathbb{R}^{n_{\mathbf{A}} \times n_{\mathbf{A}}}, \\
 \langle \mathbf{B} \vec{\mathbf{u}}, \vec{\mathbf{q}} \rangle &\approx \int_{\Gamma} \nabla_{\Gamma} q \cdot \mathbf{u} ds, \quad \mathbf{B} \in \mathbb{R}^{n_{\mathbf{S}} \times n_{\mathbf{A}}}, \\
 \langle \mathbf{M}_0 \vec{\mathbf{p}}, \vec{\mathbf{q}} \rangle &\approx \int_{\Gamma} p q ds, \quad \mathbf{M}_0 \in \mathbb{R}^{n_{\mathbf{S}} \times n_{\mathbf{S}}}, \\
 \langle \mathbf{C}_n \vec{\mathbf{p}}, \vec{\mathbf{q}} \rangle &\approx \rho_p \int_{\Omega_h^{\Gamma}} \frac{\partial p}{\partial \mathbf{n}_{\Gamma}} \frac{\partial q}{\partial \mathbf{n}_{\Gamma}} dx, \quad \mathbf{C}_n \in \mathbb{R}^{n_{\mathbf{S}} \times n_{\mathbf{S}}}, \\
 \langle \mathbf{C}_{\text{full}} \vec{\mathbf{p}}, \vec{\mathbf{q}} \rangle &\approx \rho_p \int_{\Omega_h^{\Gamma}} \nabla p \cdot \nabla q dx, \quad \mathbf{C}_{\text{full}} \in \mathbb{R}^{n_{\mathbf{S}} \times n_{\mathbf{S}}},
 \end{aligned} \tag{1}$$

respectively. We use notations as in [2], in particular, Ω_h^{Γ} is the domain consisting of tetrahedra cut by the surface $\Gamma := \{\mathbf{x} \in \mathbb{R}^3 : \phi(\mathbf{x}) = 0\}$. Here $\vec{\mathbf{u}}$ denotes a vector of d.o.f. corresponding to a FE interpolant \mathbf{u} (analogously for $\vec{\mathbf{p}}$ and p). See (5) and (6) for the computational details. Mesh-dependent parameters τ , ρ_u , and ρ_p are chosen to be proportional to some power of $h :=$ the typical mesh size for tetrahedra from Ω_h^{Γ} . Γ is chosen either as the unit sphere or torus, $\Gamma = \Gamma_{\text{sph}}$ or $\Gamma = \Gamma_{\text{tor}}$ (see Figure 1). The background domain is chosen as a cube $\Omega := (-5/3, 5/3)^3$.

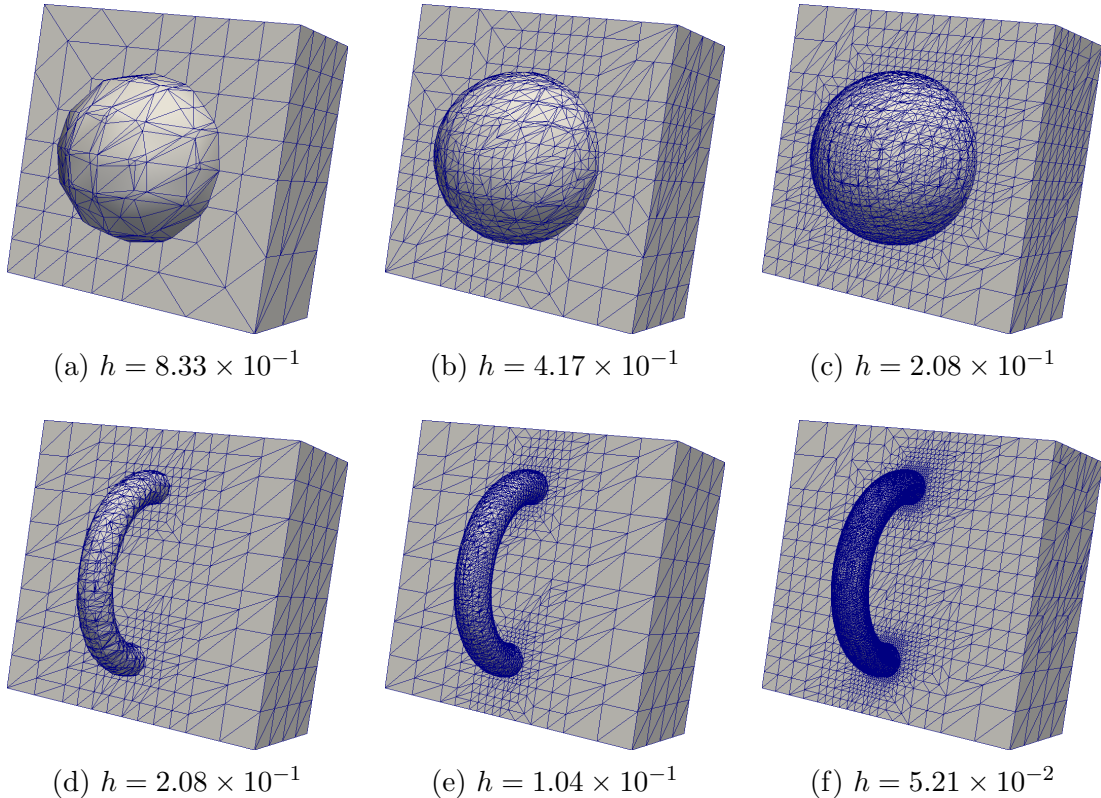


Figure 1: First three mesh levels for Γ_{sph} (top) and Γ_{tor} (bottom)

1.2 Quadratures for bilinear forms. We denote by $P_h^n \subset \bar{P}_h^n$ spaces of continuous and discontinuous nodal P_n interpolants defined on Ω_Γ^h , respectively. For a function f , $I_h^n(f) \in P_h^n$ is the corresponding interpolant; we will use the notation f_h^n to emphasize that $f_h^n \in P_h^n$ and f_h^n approximates f in some sense, but $I_h^n(f) \neq f_h^n$.

We set

$$\Gamma_h^n := \{\mathbf{x} \in \mathbb{R}^3 : (I_h^n(\phi))(\mathbf{x}) = 0\}, \quad (2)$$

$$\mathbf{n}_{\Gamma_h^n} = \frac{\nabla I_h^n(\phi)}{\|\nabla I_h^n(\phi)\|} \notin \bar{P}_h^m \text{ for any } m \text{ if } n > 1. \quad (3)$$

Note that Γ_h^n is a continuous piecewise P_n surface in Ω_Γ^h , and $\Gamma_h^n \neq I_h^n(\Gamma)$. The unit normal $\mathbf{n}_{\Gamma_h^n}$ is not a rational function; it is continuous in $T \in \Omega_\Gamma^h$ and discontinuous on faces. We also define

$$\Gamma_{h/m}^{2 \rightarrow 1} := \{\mathbf{x} \in \mathbb{R}^3 : (I_{h/m}^1(I_h^2(\phi)))(\mathbf{x}) = 0\}. \quad (4)$$

Note that $I_{h/2}^1(I_h^2(\phi)) = I_{h/2}^1(\phi)$ (since in order to build both $I_{h/2}^1$ and I_h^2 the same values of ϕ are used), and $I_{h/m}^1(I_h^2(\phi)) \neq I_{h/m}^1(\phi)$ for $m > 2$. Thus we have $\Gamma_{h/2}^{2 \rightarrow 1} = \Gamma_{h/2}^1$, and $\Gamma_{h/m}^{2 \rightarrow 1} \neq \Gamma_{h/m}^1$ for $m > 2$. We refer to Figures 2 and 3.

We implemented two options for the matrix assembly (1). The first one is

$$\begin{aligned} \langle \mathbf{A} \vec{\mathbf{u}}, \vec{\mathbf{v}} \rangle &= \int_{\Gamma_{h/m}^{2 \rightarrow 1}}^5 (2 E_{s, \Gamma_h^2}(\mathbf{u}) : E_{s, \Gamma_h^2}(\mathbf{v}) + \mathbf{u} \cdot \mathbf{v} + \tau (\mathbf{u} \cdot \mathbf{n}_{\Gamma_h^2})(\mathbf{v} \cdot \mathbf{n}_{\Gamma_h^2})) \, ds \\ &\quad + \rho_u \int_{\Omega_h^\Gamma}^5 \frac{\partial \mathbf{u}}{\partial \mathbf{n}_{\Gamma_h^2}} \cdot \frac{\partial \mathbf{v}}{\partial \mathbf{n}_{\Gamma_h^2}} \, d\mathbf{x}, \quad \mathbf{A} \in \mathbb{R}^{n_A \times n_A}, \\ \langle \mathbf{B} \vec{\mathbf{u}}, \vec{\mathbf{q}} \rangle &= \int_{\Gamma_{h/m}^{2 \rightarrow 1}}^5 \nabla_{\Gamma_h^2} q \cdot \mathbf{u} \, ds, \quad \mathbf{B} \in \mathbb{R}^{n_S \times n_A}, \\ \langle \mathbf{M}_0 \vec{\mathbf{p}}, \vec{\mathbf{q}} \rangle &= \int_{\Gamma_{h/m}^{2 \rightarrow 1}}^5 p q \, ds, \quad \mathbf{M}_0 \in \mathbb{R}^{n_S \times n_S}, \\ \langle \mathbf{C}_n \vec{\mathbf{p}}, \vec{\mathbf{q}} \rangle &= \rho_p \int_{\Omega_h^\Gamma}^5 \frac{\partial p}{\partial \mathbf{n}_{\Gamma_h^2}} \frac{\partial q}{\partial \mathbf{n}_{\Gamma_h^2}} \, d\mathbf{x}, \quad \mathbf{C}_n \in \mathbb{R}^{n_S \times n_S}, \\ \langle \mathbf{C}_{\text{full}} \vec{\mathbf{p}}, \vec{\mathbf{q}} \rangle &= \rho_p \int_{\Omega_h^\Gamma}^5 \nabla p \cdot \nabla q \, d\mathbf{x}, \quad \mathbf{C}_{\text{full}} \in \mathbb{R}^{n_S \times n_S}. \end{aligned} \quad (5)$$

- $\int_{\Gamma_{h/m}^{2 \rightarrow 1}}^5 \cdot \, ds$ denotes a composite quadrature rule that is exact for $\bar{P}_h^5(\Gamma_{h/m}^{2 \rightarrow 1})$, i.e. this quadrature is exact for piecewise polynomials up to degree 5 on each triangular patch $\gamma \in \Gamma_{h/m}^{2 \rightarrow 1}$,
- $\int_{\Omega_h^\Gamma}^5 \cdot \, d\mathbf{x}$ denotes a composite quadrature rule that is exact for $\bar{P}_h^5(\Omega_h^\Gamma)$, i.e. this quadrature is exact for piecewise polynomials up to degree 5 on each tetrahedron $T \in \Omega_h^\Gamma$,
- E_{s, Γ_h^2} and $\nabla_{\Gamma_h^2}$ are defined as their continuous analogues with \mathbf{n}_Γ in \mathbf{P}_Γ replaced with $\mathbf{n}_{\Gamma_h^2}$.

The second option is

$$\begin{aligned}
\langle \mathbf{A} \vec{\mathbf{u}}, \vec{\mathbf{v}} \rangle &= \int_{\Gamma_{h/m}^{2 \rightarrow 1}}^5 \left(2 E_{s, \Gamma_{h/m}^{2 \rightarrow 1}}(\mathbf{u}) : E_{s, \Gamma_{h/m}^{2 \rightarrow 1}}(\mathbf{v}) + \mathbf{u} \cdot \mathbf{v} + \tau (\mathbf{u} \cdot \mathbf{n}_{\Gamma_h^2}) (\mathbf{v} \cdot \mathbf{n}_{\Gamma_h^2}) \right) ds \\
&\quad + \rho_u \int_{\Omega_h^\Gamma} \frac{\partial \mathbf{u}}{\partial \mathbf{n}_{\Gamma_h^2}} \cdot \frac{\partial \mathbf{v}}{\partial \mathbf{n}_{\Gamma_h^2}} d\mathbf{x}, \quad \mathbf{A} \in \mathbb{R}^{n_A \times n_A}, \\
\langle \mathbf{B} \vec{\mathbf{u}}, \vec{\mathbf{q}} \rangle &= \int_{\Gamma_{h/m}^{2 \rightarrow 1}}^5 \nabla_{\Gamma_{h/m}^{2 \rightarrow 1}} q \cdot \mathbf{u} ds, \quad \mathbf{B} \in \mathbb{R}^{n_S \times n_A}, \\
\langle \mathbf{M}_0 \vec{\mathbf{p}}, \vec{\mathbf{q}} \rangle &= \int_{\Gamma_{h/m}^{2 \rightarrow 1}}^5 p q ds, \quad \mathbf{M}_0 \in \mathbb{R}^{n_S \times n_S}, \\
\langle \mathbf{C}_n \vec{\mathbf{p}}, \vec{\mathbf{q}} \rangle &= \rho_p \int_{\Omega_h^\Gamma} \frac{\partial p}{\partial \mathbf{n}_{\Gamma_h^2}} \frac{\partial q}{\partial \mathbf{n}_{\Gamma_h^2}} d\mathbf{x}, \quad \mathbf{C}_n \in \mathbb{R}^{n_S \times n_S}, \\
\langle \mathbf{C}_{\text{full}} \vec{\mathbf{p}}, \vec{\mathbf{q}} \rangle &= \rho_p \int_{\Omega_h^\Gamma} \nabla p \cdot \nabla q d\mathbf{x}, \quad \mathbf{C}_{\text{full}} \in \mathbb{R}^{n_S \times n_S}.
\end{aligned} \tag{6}$$

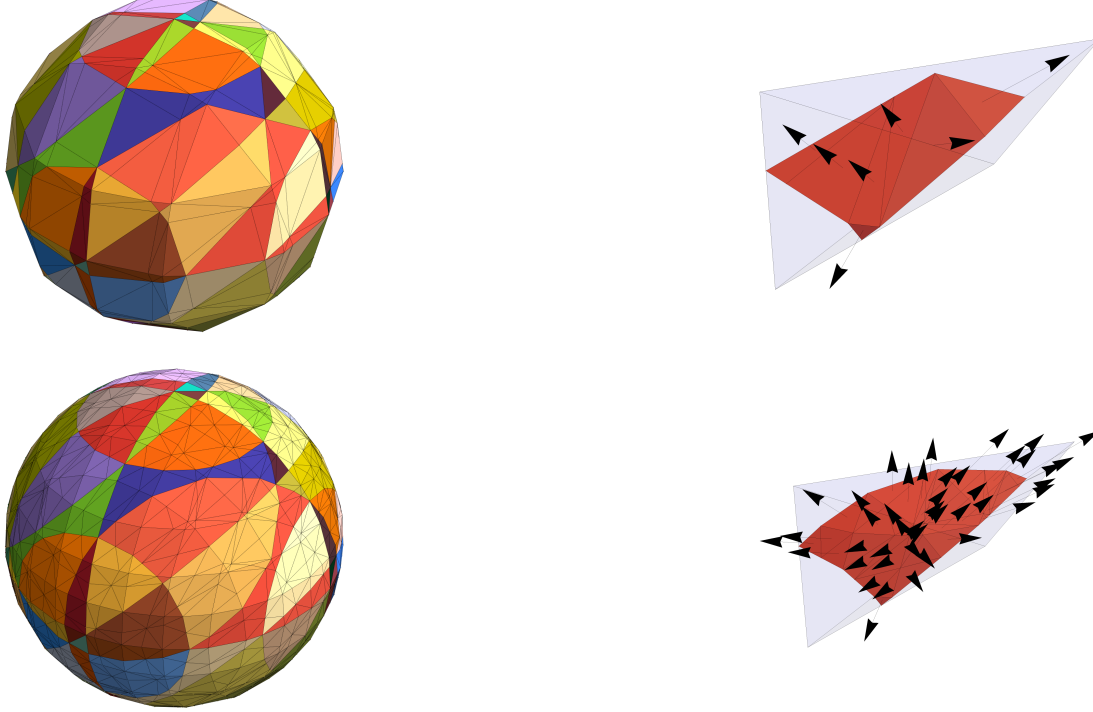


Figure 2: $\Gamma = \Gamma_{\text{sph}}$, $\phi(\mathbf{x}) = \|\mathbf{x}\|^2 - 1$, $h = 8.33 \times 10^{-1}$. Top-left: triangular patches $\gamma \in \Gamma_{h/2}^{2 \rightarrow 1} = \Gamma_{h/2}^1$ (different color corresponds to a different tetrahedron $T \in \Omega_h^\Gamma$). Top-right: a patch γ and its normals. Bottom-left and bottom-right: same for $\Gamma_{h/4}^{2 \rightarrow 1} = \Gamma_{h/4}^1$. **Note that since $\phi \in P^2$, we have that $\Gamma_{h/m}^{2 \rightarrow 1} = \Gamma_{h/m}^1 \rightarrow \Gamma$ as $m \rightarrow \infty$ even for fixed h**

For both formulations (5) and (6) the loading vectors for moments and continuity equations are approximated

as

$$\begin{aligned}\mathbf{f}_i &= \int_{\Gamma_{h/m}^{2 \rightarrow 1}}^5 \mathbf{f} \cdot \phi_i \, ds, \quad i = 1, 2, \dots, n_{\mathbf{A}}, \\ \mathbf{g}_i &= - \int_{\Gamma_{h/m}^{2 \rightarrow 1}}^5 g \phi_i \, ds, \quad i = 1, 2, \dots, n_{\mathbf{S}},\end{aligned}\tag{7}$$

respectively. Here ϕ_i and ϕ_i are vector and scalar Lagrange basis functions defined on Ω_h^Γ .



Figure 3: $\Gamma = \Gamma_{\text{sph}}$, $\phi(\mathbf{x}) = \|\mathbf{x}\|^{1/2} - 1$, $h = 8.33 \times 10^{-1}$. Left: triangular patches $\gamma \in \Gamma_{h/2}^1$ (different color corresponds to a different tetrahedron $T \in \Omega_h^\Gamma$). Right: same for $\Gamma_{h/4}^{2 \rightarrow 1} \neq \Gamma_{h/4}^1$. **Note that since** $\phi \notin \bar{P}_h^2$, **we have that** $\Gamma_{h/m}^{2 \rightarrow 1} \neq \Gamma_{h/m}^1$ **for** $m > 2$, **and** $\Gamma_{h/m}^{2 \rightarrow 1} \rightarrow \Gamma_h^2 \neq \Gamma$ **as** $m \rightarrow \infty$ **for fixed** h

As in [1], we refer to (1) as **inconsistent formulation**. We also consider the same formulation as in (1) but with the first term \mathbf{A}_s in the definition of \mathbf{A} changed as

$$\langle \mathbf{A}_s \vec{\mathbf{u}}, \vec{\mathbf{v}} \rangle \approx \int_{\Gamma} 2(E_{s,\Gamma}(\mathbf{u}) - (\mathbf{u} \cdot \mathbf{n}_{\Gamma}) \mathbf{H}_{\Gamma}) : (E_{s,\Gamma}(\mathbf{v}) - (\mathbf{v} \cdot \mathbf{n}_{\Gamma}) \mathbf{H}_{\Gamma}) \, ds, \tag{8}$$

where the shape operator is defined as $\mathbf{H}_{\Gamma} := \nabla_{\Gamma} \mathbf{n}_{\Gamma} := \mathbf{P}_{\Gamma} \nabla \mathbf{n}_{\Gamma}^e \mathbf{P}_{\Gamma}$, $\mathbf{H}_{\Gamma} : \mathcal{O}(\Gamma) \rightarrow \mathbb{R}^3$. We refer to (8) as **consistent formulation**.

Similarly to (5) and (6), we consider two discretizations of (8):

$$\langle \mathbf{A}_s \vec{\mathbf{u}}, \vec{\mathbf{v}} \rangle = \int_{\Gamma_{h/m}^{2 \rightarrow 1}}^5 2(E_{s,\Gamma_h^2}(\mathbf{u}) - (\mathbf{u} \cdot \mathbf{n}_{\Gamma_h^2}) \mathbf{H}_{\Gamma_h^2}) : (E_{s,\Gamma_h^2}(\mathbf{v}) - (\mathbf{v} \cdot \mathbf{n}_{\Gamma_h^2}) \mathbf{H}_{\Gamma_h^2}) \, ds \tag{9}$$

and

$$\langle \mathbf{A}_s \vec{\mathbf{u}}, \vec{\mathbf{v}} \rangle = \int_{\Gamma_{h/m}^{2 \rightarrow 1}}^5 2(E_{s,\Gamma_{h/m}^{2 \rightarrow 1}}(\mathbf{u}) - (\mathbf{u} \cdot \mathbf{n}_{\Gamma_{h/m}^{2 \rightarrow 1}}) \mathbf{H}_{\Gamma_h^2}) : (E_{s,\Gamma_{h/m}^{2 \rightarrow 1}}(\mathbf{v}) - (\mathbf{v} \cdot \mathbf{n}_{\Gamma_{h/m}^{2 \rightarrow 1}}) \mathbf{H}_{\Gamma_h^2}) \, ds. \tag{10}$$

Note that $\mathbf{n}_{\Gamma} = \nabla \phi / \|\nabla \phi\|$ is defined in $\mathcal{O}(\Gamma)$, so $\nabla \mathbf{n}_{\Gamma}$ makes sense and

$$\nabla \mathbf{n}_{\Gamma} = \left(\mathbf{I} - \frac{\nabla \phi \nabla \phi^T}{\|\nabla \phi\|^2} \right) \frac{\nabla^2 \phi}{\|\nabla \phi\|} = \mathbf{P}_{\Gamma} \frac{\nabla^2 \phi}{\|\nabla \phi\|}.$$

If $\mathbf{n}_{\Gamma} = \mathbf{n}_{\Gamma}^e$, one gets

$$\mathbf{H}_{\Gamma} = \mathbf{P}_{\Gamma} \frac{\nabla^2 \phi}{\|\nabla \phi\|} \mathbf{P}_{\Gamma}. \tag{11}$$

Thus we define $\mathbf{H}_{\Gamma_h^2}$ to be as in (11) but with ϕ replaced with $I_h^2(\phi)$, i.e.

$$\mathbf{H}_{\Gamma_h^2} := \mathbf{P}_{\Gamma_h^2} \frac{\nabla^2 I_h^2(\phi)}{\|\nabla I_h^2(\phi)\|} \mathbf{P}_{\Gamma_h^2}. \quad (12)$$

Indeed, computation of $\mathbf{H}_{\Gamma_h^2}$ requires Hessians of shape functions.

Depending on the choice of ϕ , we may or may not have $\mathbf{n}_\Gamma = \mathbf{n}_\Gamma^e$. Note that the choice $\phi = d$ is sufficient for this, but not necessary. Consider this choices of ϕ for Γ_{sph} :

1. $\phi_1(\mathbf{x}) = \|\mathbf{x}\| - 1 = d(\mathbf{x})$, $\nabla\phi_1/\|\nabla\phi_1\| = \mathbf{n}_\Gamma^e$,
2. $\phi_2(\mathbf{x}) = \|\mathbf{x}\|^2 - 1 \in P^2$, $\nabla\phi_2/\|\nabla\phi_2\| = \nabla\phi_1/\|\nabla\phi_1\| = \mathbf{n}_\Gamma^e$,
3. $\phi_3(\mathbf{x}) = e^{\phi_2(\mathbf{x})} x^2 + y^2 + z^2 - 1$, $\nabla\phi_3/\|\nabla\phi_3\| \neq \mathbf{n}_\Gamma^e$, i.e. $\nabla\phi_3/\|\nabla\phi_3\| = \mathbf{n}_\Gamma$ only on Γ_{sph} .

As for the case 2: note that if ϕ is piecewise quadratic in Ω_h^Γ and defines a normal that is equal to its extension, then $\mathbf{H}_{\Gamma_h^2} = \mathbf{H}_\Gamma$, i.e. the approximation is **exact**.

For the approach (6), there is also an option to approximate \mathbf{H} as $\mathbf{P}_{\Gamma_{h/m}^{2 \rightarrow 1}} \frac{\nabla^2 I_h^2(\phi)}{\|\nabla I_h^2(\phi)\|} \mathbf{P}_{\Gamma_{h/m}^{2 \rightarrow 1}}$ since we build $\mathbf{P}_{\Gamma_{h/m}^{2 \rightarrow 1}}$ anyway. We chose to use (12) for both (5) and (6).

1.3 Error computation. Note that $\mathbb{H}^1(\Gamma)$ -error (for e.g. $\mathbf{P}_2 - P_1$ FE) can be cheaply approximated as $\langle \mathbf{w}, \mathbf{A}_s \mathbf{w} \rangle^{1/2}$ where $\mathbf{w} :=$ vector of d.o.f. corresponding to \mathbf{P}_h^2 interpolant $I_h^2(\mathbf{u}^e) - \mathbf{u}_h$, $\mathbf{A}_s :=$ matrix corresponding to the first term of \mathbf{A} in (6). Thus the errors are approximated as

$$\begin{aligned} \|\mathbf{u} - \mathbf{u}_h\|_{\mathbb{H}^1(\Gamma)} &= \|I_h^k(\mathbf{u}^e) - \mathbf{u}_h\|_{\mathbb{H}^1(\Gamma_{h/m}^{2 \rightarrow 1})} + O(h^k), \\ \|\mathbf{u} - \mathbf{u}_h\|_{\mathbb{L}^2(\Gamma)} &= \|I_h^k(\mathbf{u}^e) - \mathbf{u}_h\|_{\mathbb{L}^2(\Gamma_{h/m}^{2 \rightarrow 1})} + O(h^{k+1}), \\ \|p - p_h\|_{\mathbb{L}^2(\Gamma)} &= \|I_h^1(p^e) - p_h\|_{\mathbb{L}^2(\Gamma_{h/m}^{2 \rightarrow 1})} + O(h^2) \end{aligned} \quad (13)$$

for $m > 1$. Here $k = 1$ for $\mathbf{P}_1 - P_1$ FEM and $k = 2$ for $\mathbf{P}_2 - P_1$. For consistent penalty approach matrix \mathbf{A}_s is computed as in (9) or (10).

2 Convergence results

2.1 Manufactured solution. We solve model problem from [2, p. 20], $\Gamma = \Gamma_{\text{sph}}$ ¹. We set

$$\tilde{\mathbf{u}}(x, y, z) := (-z^2, y, x)^T, \quad \tilde{p}(x, y, z) := x y^2 + z, \quad \phi(\mathbf{x}) := \|\mathbf{x}\|^2 - 1. \quad (14)$$

The exact solution on the unit sphere is chosen as

$$\mathbf{u} := \mathbf{P}_\Gamma \tilde{\mathbf{u}}^e, \quad p := \tilde{p}^e. \quad (15)$$

Thus we have $\int_\Gamma p \, d\mathbf{x} = 0$, $p \equiv p^e$, $\mathbf{u} \equiv \mathbf{u}^e$ in $\mathcal{O}(\Gamma)$, and \mathbf{u} is a tangential field. Note that for our choice of ϕ in (14) we have

$$\mathbf{n}_{\Gamma_h^2} = \mathbf{n}_\Gamma^e \text{ in } \mathcal{O}(\Gamma), \quad \Gamma_{h/m}^{2 \rightarrow 1} = \Gamma_{h/m}^1, \quad \mathbf{n}_{\Gamma_{h/m}^{2 \rightarrow 1}} = \mathbf{n}_{\Gamma_{h/m}^1} \text{ on } \Gamma, \quad (16)$$

and

$$\mathbf{n}_{\Gamma_{h/m}^1} \rightarrow \mathbf{n}_\Gamma, \quad \Gamma_{h/m}^1 \rightarrow \Gamma \quad (17)$$

as one increases m even for fixed h .

¹In [2] they use $\mathbf{u} := \mathbf{P} \tilde{\mathbf{u}}$, i.e. $\mathbf{u} \neq \mathbf{u}^e$. I prefer $\mathbf{u} \equiv \mathbf{u}^e$ as in [1].

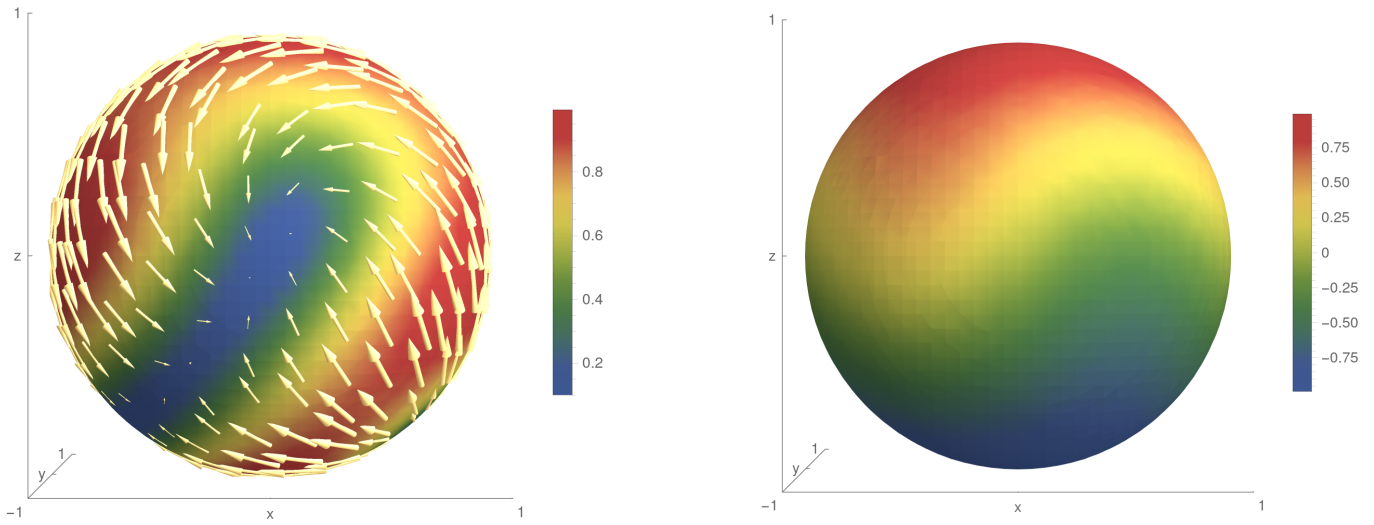


Figure 4: Exact velocity solution (Left) and pressure solution (Right) as in (15)

We have

$$\mathbf{n}_{\Gamma_{\text{sph}}}(\mathbf{x}) = \|\mathbf{x}\|^{-1} \mathbf{x} = \mathbf{n}_{\Gamma_{\text{sph}}}^e(\mathbf{x}), \quad (18)$$

$$\mathbf{P}_{\Gamma_{\text{sph}}}(\mathbf{x}) = \|\mathbf{x}\|^{-2} \begin{pmatrix} y^2 + z^2 & -xy & -xz \\ -xy & x^2 + z^2 & -yz \\ -xz & -yz & x^2 + y^2 \end{pmatrix} = \mathbf{P}_{\Gamma_{\text{sph}}}^e(\mathbf{x}), \quad (19)$$

$$\mathbf{H}_{\Gamma_{\text{sph}}}(\mathbf{x}) = \|\mathbf{x}\|^{-3} \begin{pmatrix} y^2 + z^2 & -xy & -xz \\ -xy & x^2 + z^2 & -yz \\ -xz & -yz & x^2 + y^2 \end{pmatrix} \neq \mathbf{H}_{\Gamma_{\text{sph}}}^e(\mathbf{x}) = \mathbf{P}_{\Gamma_{\text{sph}}}(\mathbf{x}). \quad (20)$$

We consider two choices for virtual refinement: $m \propto h^{-1/2}$ and $m \propto h^{-1}$. The first choice assures h^3 -accurate approximation of Γ and $h^{3/2}$ accurate approximation of the normal vector, whereas the second choice assures h^4 - and h^2 -approximations. We refer to Figure 5.

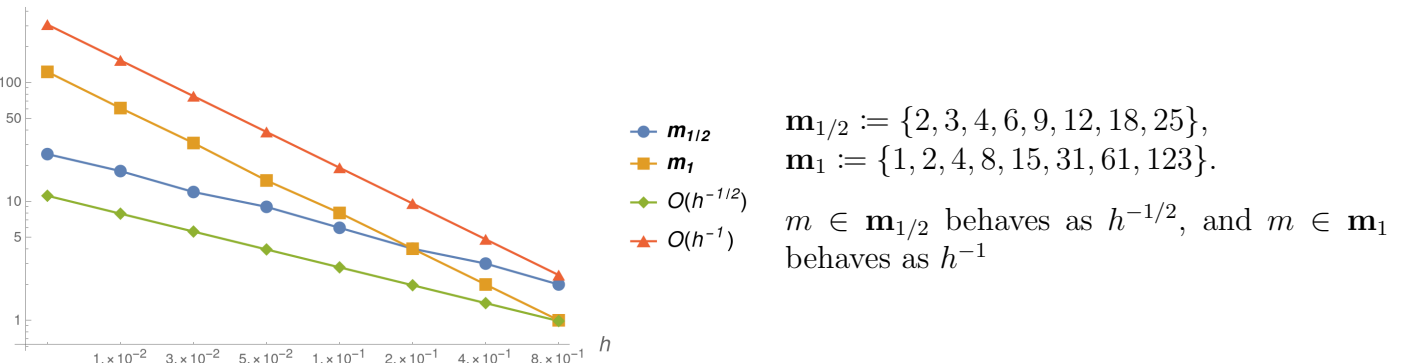


Figure 5: Virtual refinement parameter m for $\Gamma_{h/m}^{2 \rightarrow 1}$

Table 1: Errors for normals and shape operator. Please see (16) and (17)

$m \in \mathbf{m}_{1/2}$ as in Figure 5					
h	$\ \mathbf{n}_\Gamma^e - \mathbf{n}_{\Gamma_h^2}\ _{\mathbb{L}^2(\Gamma_h^1)}$	$\ \mathbf{n}_\Gamma^e - \mathbf{n}_{\Gamma_{h/m}^1}\ _{\mathbb{L}^2(\Gamma_{h/m}^1)}$	Order	$\ \mathbf{H}_\Gamma^e - \mathbf{H}_{\Gamma_h^2}\ _{\mathbb{L}^2(\Gamma_h^1)}$	Order
8.3×10^{-1}	8.1×10^{-16}	6.4×10^{-1}		2.3×10^{-1}	
4.2×10^{-1}	1.1×10^{-15}	$2. \times 10^{-1}$	1.7	2.5×10^{-2}	3.2
2.1×10^{-1}	2.3×10^{-15}	7.6×10^{-2}	1.4	3.5×10^{-3}	2.8
$1. \times 10^{-1}$	5.2×10^{-15}	2.5×10^{-2}	1.6	3.9×10^{-4}	3.2
5.2×10^{-2}	9.3×10^{-15}	8.4×10^{-3}	1.6	4.3×10^{-5}	3.2
2.6×10^{-2}	1.9×10^{-14}	3.1×10^{-3}	1.4	6.1×10^{-6}	2.8

2.2 $P_2 - P_1$ Trace FEM. Next we compare inconsistent and consistent Trace FEM penalty formulations.

2.2.1 Inconsistent penalty formulation. We use the normal stabilization matrix \mathbf{C}_n . We stick to the approach (5), so with (16) we have

$$\begin{aligned}
\langle \mathbf{A} \vec{\mathbf{u}}, \vec{\mathbf{v}} \rangle &= \int_{\Gamma_{h/2}^1}^5 (2 E_{s,\Gamma}(\mathbf{u}) : E_{s,\Gamma}(\mathbf{v}) + \mathbf{u} \cdot \mathbf{v} + \tau (\mathbf{u} \cdot \mathbf{n}_\Gamma) (\mathbf{v} \cdot \mathbf{n}_\Gamma)) \, ds \\
&\quad + \rho_u \int_{\Omega_h^\Gamma}^5 \frac{\partial \mathbf{u}}{\partial \mathbf{n}_\Gamma} \cdot \frac{\partial \mathbf{v}}{\partial \mathbf{n}_\Gamma} \, d\mathbf{x}, \quad \mathbf{A} \in \mathbb{R}^{n_A \times n_A}, \\
\langle \mathbf{B} \vec{\mathbf{u}}, \vec{\mathbf{q}} \rangle &= \int_{\Gamma_{h/2}^1}^5 \nabla_\Gamma q \cdot \mathbf{u} \, ds, \quad \mathbf{B} \in \mathbb{R}^{n_S \times n_A}, \\
\langle \mathbf{M}_0 \vec{\mathbf{p}}, \vec{\mathbf{q}} \rangle &= \int_{\Gamma_{h/2}^1}^5 p q \, ds, \quad \mathbf{M}_0 \in \mathbb{R}^{n_S \times n_S}, \\
\langle \mathbf{C}_n \vec{\mathbf{p}}, \vec{\mathbf{q}} \rangle &= \rho_p \int_{\Omega_h^\Gamma}^5 \frac{\partial p}{\partial \mathbf{n}_\Gamma} \frac{\partial q}{\partial \mathbf{n}_\Gamma} \, d\mathbf{x}, \quad \mathbf{C}_n \in \mathbb{R}^{n_S \times n_S}.
\end{aligned} \tag{21}$$

Table 2: Convergence results. $\tau = h^{-2}$, $\rho_u = h$, $\rho_p = h$. Matrices are assembled as in (21)

$m \in \mathbf{m}_{1/2}$ as in Figure 5						
h	$\ \mathbf{u} - \mathbf{u}_h\ _{\mathbb{H}^1}$	Order	$\ \mathbf{u} - \mathbf{u}_h\ _{\mathbb{L}^2}$	Order	$\ p - p_h\ _{\mathbb{L}^2}$	Order
8.3×10^{-1}	3.		1.8		2.1	
4.2×10^{-1}	1.8	7.4×10^{-1}	9.1×10^{-1}	9.7×10^{-1}	1.7	2.7×10^{-1}
2.1×10^{-1}	$7. \times 10^{-1}$	1.4	3.4×10^{-1}	1.4	6.9×10^{-1}	1.3
$1. \times 10^{-1}$	$2. \times 10^{-1}$	1.8	9.9×10^{-2}	1.8	$2. \times 10^{-1}$	1.8
5.2×10^{-2}	5.2×10^{-2}	1.9	2.6×10^{-2}	1.9	5.2×10^{-2}	1.9
2.6×10^{-2}	1.3×10^{-2}	2.	6.5×10^{-3}	2.	1.3×10^{-2}	2.

h	$\ \mathbf{u}_h \cdot \mathbf{n}\ _{\mathbb{L}^2}$	Order	Outer iterations	Residual norm
8.33×10^{-1}	1.8		24	6.2×10^{-9}
4.17×10^{-1}	9.2×10^{-1}	9.4×10^{-1}	31	5.4×10^{-9}
2.08×10^{-1}	3.5×10^{-1}	1.4	30	9.8×10^{-9}
1.04×10^{-1}	9.9×10^{-2}	1.8	27	7.8×10^{-9}
5.21×10^{-2}	2.6×10^{-2}	1.9	26	8.3×10^{-9}

For statistics: using 64 CPUs, computation of the meshlevel 3 ($h = 2.08 \times 10^{-1}$) takes ~ 1 minute, meshlevel 4 takes ~ 7 minutes, meshlevel 5 takes ~ 50 minutes, meshlevel 6 takes 4.8 hours, and meshlevel 7 takes ~ 21.3 hours.

2.2.2 Consistent penalty formulation. We consider the same formulation as in (21), but with the first \mathbf{A}_s term in the definition of \mathbf{A} changed according to (9). Thus with (16) we have

$$\langle \mathbf{A}_s \vec{\mathbf{u}}, \vec{\mathbf{v}} \rangle = \int_{\Gamma_{h/m}^1}^5 2(E_{s,\Gamma}(\mathbf{u}) - (\mathbf{u} \cdot \mathbf{n}_\Gamma) \mathbf{H}_\Gamma) : (E_{s,\Gamma}(\mathbf{v}) - (\mathbf{v} \cdot \mathbf{n}_\Gamma) \mathbf{H}_\Gamma) \, ds. \quad (22)$$

Table 3: Convergence results. $\tau = h^{-2}$, $\rho_u = h^{-1}$, $\rho_p = h$. Matrices are assembled as in (21)–(22)

$m \in \mathbf{m}_{1/2}$ as in Figure 5						
h	$\ \mathbf{u} - \mathbf{u}_h\ _{\mathbb{H}^1}$	Order	$\ \mathbf{u} - \mathbf{u}_h\ _{\mathbb{L}^2}$	Order	$\ p - p_h\ _{\mathbb{L}^2}$	Order
8.3×10^{-1}	1.2		4.8×10^{-1}		4.2×10^{-1}	
4.2×10^{-1}	3.7×10^{-1}	1.8	6.1×10^{-2}	3.	1.1×10^{-1}	2.
2.1×10^{-1}	9.2×10^{-2}	2.	5.8×10^{-3}	3.4	2.5×10^{-2}	2.1
$1. \times 10^{-1}$	2.2×10^{-2}	2.1	5.6×10^{-4}	3.4	6.3×10^{-3}	2.
5.2×10^{-2}	5.4×10^{-3}	2.	5.2×10^{-5}	3.4	1.7×10^{-3}	1.8
2.6×10^{-2}	1.4×10^{-3}	2.	5.4×10^{-6}	3.3	5.3×10^{-4}	1.7

h	$\ \mathbf{u}_h \cdot \mathbf{n}\ _{\mathbb{L}^2}$	Order	Outer iterations	Residual norm
8.33×10^{-1}	3.4×10^{-1}		26	7.3×10^{-9}
4.17×10^{-1}	5.3×10^{-2}	2.7	33	4.8×10^{-9}
2.08×10^{-1}	4.9×10^{-3}	3.4	31	$6. \times 10^{-9}$
1.04×10^{-1}	$5. \times 10^{-4}$	3.3	27	8.3×10^{-9}
5.21×10^{-2}	4.9×10^{-5}	3.4	26	8.6×10^{-9}
2.6×10^{-2}	$5. \times 10^{-6}$	3.3	26	7.5×10^{-9}

For statistics: using 80 CPUs, computation of the meshlevel 7 ($h = 1.3 \times 10^{-2}$) takes ~ 74.3 hours with $m = 64$ (computation also involves errors for normals and the shape operator).

3 Inf-sup stability: pressure Schur complement generalized eigenvalues

3.1 Solution description. We define matrices

$$\mathbf{C}_0 := \mathbf{0}, \quad \mathbf{M}_n := \mathbf{M}_0 + \mathbf{C}_n, \quad \mathbf{M}_{\text{full}} := \mathbf{M}_0 + \mathbf{C}_{\text{full}}. \quad (23)$$

We are interested in (generalized) extreme eigenvalues of the pressure Schur complement matrices

$$\mathbf{S}_0 := \mathbf{B} \mathbf{A}^{-1} \mathbf{B}^T, \quad \mathbf{S}_n := \mathbf{S}_0 + \mathbf{C}_n, \quad \mathbf{S}_{\text{full}} := \mathbf{S}_0 + \mathbf{C}_{\text{full}}, \quad (24)$$

i.e. in solving

$$\mathbf{S}_\star \mathbf{x} = \lambda \mathbf{M}_\star \mathbf{x}, \quad (25)$$

where “ \star ” stands for “0,” “ n ,” or “full.” We denote by $0 = \lambda_1 < \lambda_2 \leq \dots \leq \lambda_{ns} = O(1)$ the spectrum of (25).

Computing \mathbf{A}^{-1} in (24) becomes troublesome already for $h = 5.21 \times 10^{-2}$ ($n_{\mathbf{A}} = 32736$ for $\mathbf{u} \in \mathbf{P}_1$ FE space): although \mathbf{A} is sparse, \mathbf{A}^{-1} is dense and consumes 8.5+ GB in double-precision arithmetic. A quick research showed that Mathematica has no built-in matrix-free eigenvalue routines. Intel MKL's FEAST algorithm for computing (generalized) eigenvalues in an interval is suitable for matrix-free implementations; however, it requires some expensive operations to be implemented (e.g. matrix-matrix multiplications $\mathbf{Y} \leftarrow \mathbf{S}_* \mathbf{X}$, $\mathbf{Y} \leftarrow \mathbf{M}_* \mathbf{X}$ and approximating the action of inverses in the form $\mathbf{y} \leftarrow (\sigma \mathbf{M}_* - \mathbf{S}_*)^{-1} \mathbf{x}$).

Taking this into account, instead of (25) we consider a perturbed² problem

$$\underbrace{\begin{bmatrix} \mathbf{A} & \mathbf{B}^T \\ \mathbf{B} & -\mathbf{C}_* \end{bmatrix} \begin{bmatrix} \mathbf{x} \\ \mathbf{y} \end{bmatrix}}_{\mathcal{A}_* :=} = \mu \underbrace{\begin{bmatrix} \epsilon \mathbf{A} & \\ & \mathbf{M}_* \end{bmatrix} \begin{bmatrix} \mathbf{x} \\ \mathbf{y} \end{bmatrix}}_{\mathcal{M}_*^\epsilon :=} \quad (26)$$

with $0 < \epsilon \ll 1$. For \mathcal{A}_0 and \mathcal{M}_0^ϵ we have

$$\mu = -\lambda + o(1) \quad \text{or} \quad \epsilon^{-1} + \lambda + o(1), \quad \epsilon \rightarrow 0. \quad (27)$$

This makes it easy to pick only “correct” eigenvalues. To ease the computation further we replace the $(1, 1)$ -block of \mathcal{M}_*^ϵ with $\epsilon \mathbf{I}$.

To make sure that results are consistent we solve (26) for $\epsilon = 10^{-5}$ and $\epsilon = 10^{-6}$; for the coarse mesh levels we also check that the dense solver for (25) and the iterative one for (26) give solutions that coincide.

²The majority of generalized eigenvalue solvers require left-hand-side matrix to be Hermitian and right-hand-side matrix to be Hermitian **positive definite**; that's why we need to introduce $\epsilon > 0$.

3.2 Dependency of the spectrum on the mesh size. Here we test inconsistent $\mathbf{P}_1 - P_1$, inconsistent $\mathbf{P}_2 - P_1$, and consistent $\mathbf{P}_2 - P_1$ approaches.

Table 4: Spectrum of (25) for inconsistent $\mathbf{P}_1 - P_1$, $\tau = h^{-2}$, $\rho_u = h$, $\rho_p = h$, $m \equiv 2$

(a) $\Gamma = \Gamma_{\text{sph}}$

h	$n_{\mathbf{A}}$	$n_{\mathbf{S}}$	\mathbf{S}_0		\mathbf{S}_n		\mathbf{S}_{full}	
			λ_2	$\lambda_{n_{\mathbf{S}}}$	λ_2	$\lambda_{n_{\mathbf{S}}}$	λ_2	$\lambda_{n_{\mathbf{S}}}$
8.33×10^{-1}	153	51	1.32×10^{-2}	1.42	7.48×10^{-1}	1.13	9.58×10^{-1}	1.06
4.17×10^{-1}	570	190	5.12×10^{-3}	1.04	5.77×10^{-1}	1.	8.54×10^{-1}	1.
2.08×10^{-1}	1992	664	4.4×10^{-3}	7.93×10^{-1}	3.87×10^{-1}	1.	6.71×10^{-1}	1.
1.04×10^{-1}	8292	2764	2.01×10^{-3}	7.79×10^{-1}	2.19×10^{-1}	1.	5.82×10^{-1}	1.
5.21×10^{-2}	32736	10912	6.04×10^{-5}	9.81×10^{-1}	1.17×10^{-1}	1.	5.37×10^{-1}	1.
2.6×10^{-2}	131592	43864	3.53×10^{-5}	8.67×10^{-1}	5.72×10^{-2}	1.	5.16×10^{-1}	1.
1.3×10^{-2}	525864	175288	2.16×10^{-6}	7.34×10^{-1}	2.84×10^{-2}	1.	5.04×10^{-1}	1.

(b) $\Gamma = \Gamma_{\text{tor}}$

h	$n_{\mathbf{A}}$	$n_{\mathbf{S}}$	\mathbf{S}_0		\mathbf{S}_n		\mathbf{S}_{full}	
			λ_2	$\lambda_{n_{\mathbf{S}}}$	λ_2	$\lambda_{n_{\mathbf{S}}}$	λ_2	$\lambda_{n_{\mathbf{S}}}$
2.08×10^{-1}	972	324	5.04×10^{-2}	4.93	2.84×10^{-1}	1.35	3.64×10^{-1}	1.19
1.04×10^{-1}	4740	1580	2.99×10^{-3}	3.83	1.58×10^{-1}	1.02	3.35×10^{-1}	1.01
5.21×10^{-2}	19704	6568	1.11×10^{-3}	5.45	7.73×10^{-2}	1.01	3.25×10^{-1}	1.
2.6×10^{-2}	80808	26936	1.2×10^{-4}	5.42	3.07×10^{-2}	1.01	3.21×10^{-1}	1.
1.3×10^{-2}	327036	109012	1.77×10^{-5}	5.23	1.18×10^{-2}	1.01	3.16×10^{-1}	1.

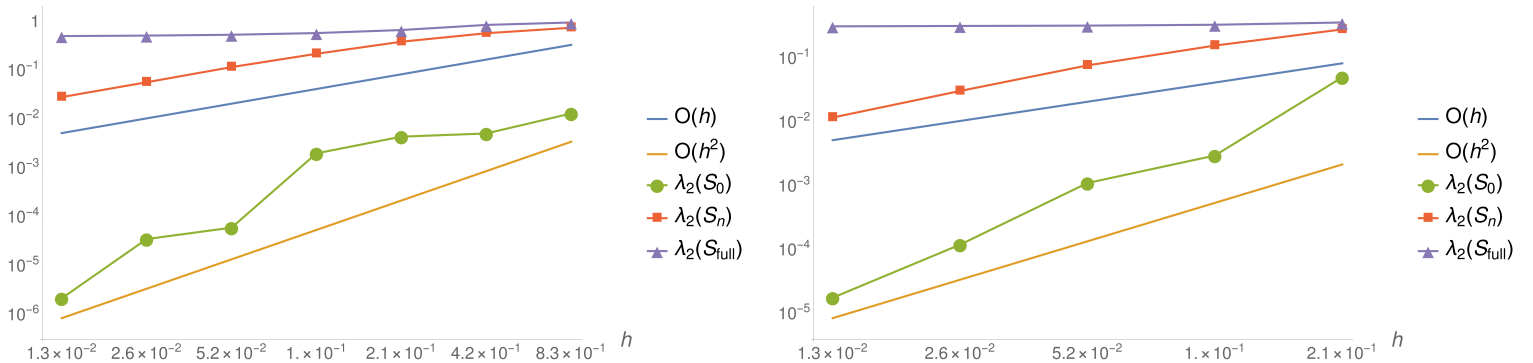


Figure 6: Log-log plot of λ_2 for Tables 4a (left) and 4b (right)

Table 5: Spectrum of (25) for consistent $\mathbf{P}_2 - P_1$, $\tau = h^{-2}$, $\rho_u = h^{-1}$, $\rho_p = h$, $m \in \mathbf{m}_{1/2}$ as in Figure 5

(a) $\Gamma = \Gamma_{\text{sph}}$

h	$n_{\mathbf{A}}$	$n_{\mathbf{S}}$	\mathbf{S}_0		\mathbf{S}_n		\mathbf{S}_{full}	
			λ_2	$\lambda_{n_{\mathbf{S}}}$	λ_2	$\lambda_{n_{\mathbf{S}}}$	λ_2	$\lambda_{n_{\mathbf{S}}}$
8.33×10^{-1}	789	51	2.33×10^{-1}	1.07	6.3×10^{-1}	1.	8.81×10^{-1}	1.
4.17×10^{-1}	3276	190	4.72×10^{-2}	6.97×10^{-1}	5.29×10^{-1}	1.	7.64×10^{-1}	1.
2.08×10^{-1}	11718	664	7.93×10^{-2}	6.7×10^{-1}	5.09×10^{-1}	1.	6.39×10^{-1}	1.
1.04×10^{-1}	48762	2764	3.71×10^{-2}	6.69×10^{-1}	5.03×10^{-1}	1.	5.73×10^{-1}	1.
5.21×10^{-2}	193086	10912	1.81×10^{-3}	6.68×10^{-1}	4.98×10^{-1}	1.	5.36×10^{-1}	1.
2.6×10^{-2}	775998	43864	6.65×10^{-4}	6.65×10^{-1}	4.92×10^{-1}	1.	5.17×10^{-1}	1.

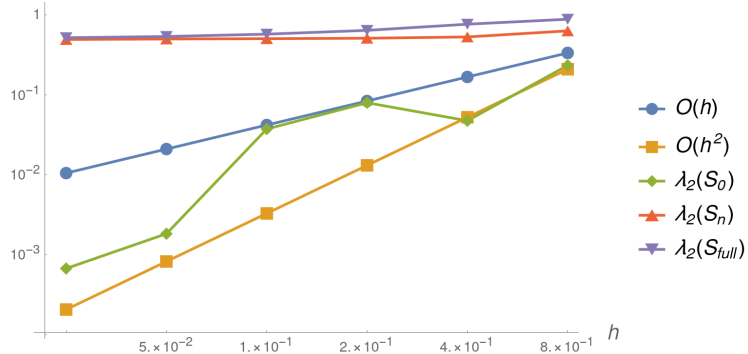


Figure 7: Log-log plot of λ_2 for Table 5a

3.3 Sensitivity of the spectrum to levelset shifts. In this section we investigate the sensitivity of the spectrum to levelset shifts

$$\Gamma \mapsto \Gamma + \alpha \mathbf{s} \quad (28)$$

for some $\alpha \in \mathbb{R}$ and $\mathbf{s} \in \mathbb{R}^3$, $\|\mathbf{s}\| = 1$. We refer to Figure 8.

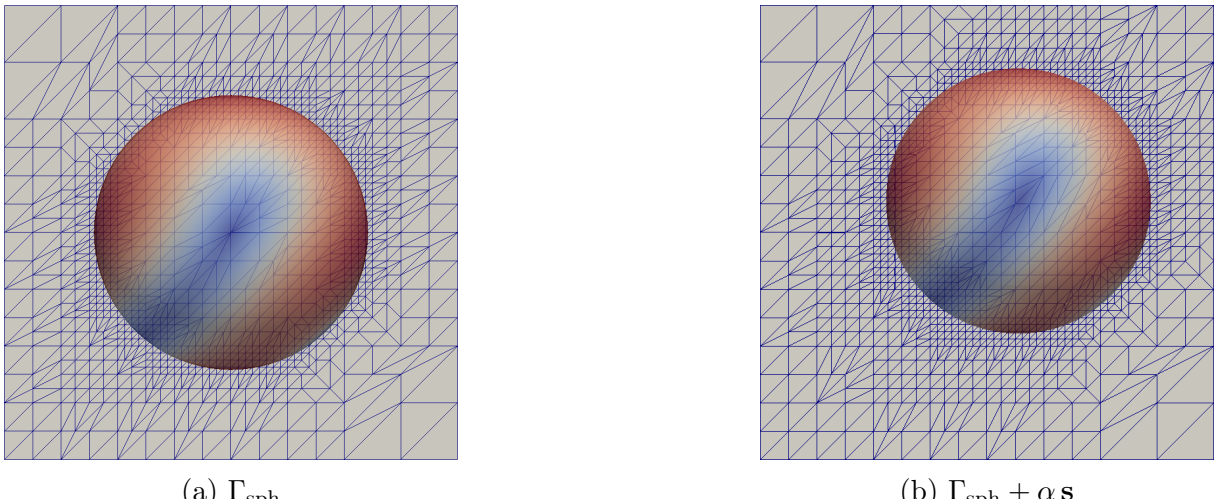


Figure 8: $\|\mathbf{u}_h\|$ on the unit sphere (left) and the shifted unit sphere (right). Here $\mathbf{s} = (1, 1, 1)^T / \sqrt{3}$, $\alpha = 0.4$, and $h = 1.04 \times 10^{-1}$

Table 6: Spectrum of (25) for perturbed levelset $\Gamma + \alpha \mathbf{s}$ for consistent $\mathbf{P}_2 - P_1$, $\tau = h^{-2}$, $\rho_u = h^{-1}$, $\rho_p = h$, $m \in \mathbf{m}_{1/2}$ as in Figure 5. Here $\mathbf{s} = (1, 1, 1)^T / \sqrt{3}$, $h = 1.04 \times 10^{-1}$

Surface	\mathbf{S}_0		\mathbf{S}_n		\mathbf{S}_{full}	
	λ_2	λ_{ns}	λ_2	λ_{ns}	λ_2	λ_{ns}
$\Gamma_{\text{sph}} + 0.0 \mathbf{s}$	3.714×10^{-2}	6.69×10^{-1}	5.03×10^{-1}	1.	5.731×10^{-1}	1.
$\Gamma_{\text{sph}} + 0.1 \mathbf{s}$	1.313×10^{-3}	6.87×10^{-1}	5.03×10^{-1}	1.	5.733×10^{-1}	1.
$\Gamma_{\text{sph}} + 0.3 \mathbf{s}$	1.036×10^{-2}	6.72×10^{-1}	5.031×10^{-1}	1.	5.73×10^{-1}	1.
$\Gamma_{\text{sph}} + 0.4 \mathbf{s}$	5.315×10^{-4}	6.72×10^{-1}	5.031×10^{-1}	1.	5.731×10^{-1}	1.

References

- [1] T. Jankuhn and A. Reusken. Trace Finite Element Methods for Surface Vector-Laplace Equations. *arXiv e-prints*, April 2019.

- [2] M. Olshanskii, A. Quaini, A. Reusken, and V. Yushutin. A finite element method for the surface stokes problem. *SIAM Journal on Scientific Computing*, 40(4):A2492–A2518, 2018.